Investigation of tunneling effects modeling in degenerate semiconductors

A. Karkri[1], A. Chetouani[2], D. Moussaid [1], S. E. Elqebbaj[1], M. Benaichi[1]

[1]*Electronic & System Laboratory, Faculty of Sciences, Mohammed First University, Oujda 60500   Morocco*
[2]*Laboratory of Stochastic & Deterministic Modelling, Faculty of Sciences, Mohammed First University, Oujda 60500   Morocco*

Abstract

Tunneling effect is an important process in degenerate semiconductors, especially when the electrical field in space charge regions is very strong (upper than 10^9 V.cm^{-1}) and doping is higher (upper than 10^{19} cm^{-3}). This paper provides a detailed description of tunneling mechanisms in a multi-junction structure. It takes into account the band-to-band tunneling effect and the traps-assisted tunneling process through discrete states located in the bandgap. The numerical algorithm is based on a one-dimensional steady state drift diffusion model and uses the Fermi-Dirac statistics to describe carrier's transport in semiconductors. The use of this distribution leads to an integral calculation which cannot be evaluated analytically and needs special numerical methods. Our model employs also a generalized Scharfetter-Gummel discretization scheme, which is consistent with both equilibrium and non-equilibrium cases. Numerical tests have been carried out on a multi-junction structure with different levels of doping including layers with degenerate and non-degenerate semiconductors. Different parameters and electrical characterizations have been simulated to examine the contribution of these effects in the performance of the structure. It is shown that extended Scharfetter-Gummel scheme is stable convergent. On the other hand, adding tunneling effect shows the predicted peak and valley in the I-V curve.

1. Introduction

To increase solar cells efficiencies, several pn-junctions with different energy bandgap have to be stacked, in order to absorb a big part of the solar spectrum [1]. The stacking is made through tunnel junction [2], which is formed from highly doped semiconductors. Therefore, the obtained structure requires a special treatment of the transport equations and causes new current beside the standard ones (drift and diffusion currents) [3], compared to normal pn-junctions. The additional currents are due to the tunneling of carriers through the bandgap in two ways: the first one occurs on a direct way (band-to-band tunneling) and the second takes place with the help of traps in the bandgap (traps-assisted tunneling).

Several models were developed to simulate tunneling effects [4-6], but they were applied for particular structures and used the Boltzmann approximation, which is consistent only with nondegenerate semiconductors [7]. Despite these efforts, the literature is still lacking detailed simulations of multi-junction structure with a universal tunneling model, including the two mechanisms (band-to-band and traps-assisted tunneling).

Unlike three dimensional researchers [8], whose analyze the device design and lateral effects, we provide in this work a one dimensional steady state model, based on the drift-diffusion equations. To be consistent with any level of doping, our model uses a generalized Fermi-Dirac integral expression [9,10]. The Decoupling of equations is made through an extended Scharfetter-Gummel scheme [11-13], and is based on a modified Einstein relation [14]. This method allows to overcome the instability of the system and increases the opportunity of convergence [15]. Tunneling effects are included in this model via additional recombination terms in the electrons and holes continuity equations.

Numerical tests are outlined on a multi-junction structure, with different levels of doping including degenerate and non-degenerate semiconductors. Different parameters and electrical characterizations were simulated to see the contribution of tunneling effect in the performance of the device.

The rest of this paper is structured as follows: in Section 2, we introduce a model for steady-state charge transport in semiconductors. We present also the Fermi-Dirac integrals and the proper Scharfetter-Gummel scheme, accounting for the generalized Einstein relation. In the same section, we describe tunneling

mechanisms in degenerate semiconductors and how they can be incorporated in the drift-diffusion model. Numerical simulations for a GaAs tunnel junction are given in Section 3, comparing the influences of different tunneling mechanisms on the J-V curve of the simulated structure. Finally, we draw our conclusions.

2. Computational methods

2.1. *Drift-diffusion model*

In this paper, our simulations are based on a one dimensional steady state drift-diffusion model [3], in which the electron and hole current densities are treated as it is shown in equations (1) and (2).

$$J_n = k_b T \mu_n \left(g_n \frac{dn}{dx} - qn \frac{dV}{dx} \right) \tag{1}$$

$$J_p = -k_b T \mu_p \left(g_p \frac{dp}{dx} + qp \frac{dV}{dx} \right) \tag{2}$$

Where q is the elementary charge, k_b is the Boltzmann constant and V is the electrostatic potential. μ_n and μ_p refer to the mobilities of electrons and holes, respectively. These mobilities are related to the diffusion coefficients of electrons D_n and holes D_p with the equation (3), which represents a generalized expression of the Einstein relation.

$$\frac{D_{n,p}}{\mu_{n,p}} = \frac{k_b T}{q} g_{n,p} \tag{3}$$

Here, g_n and g_p represent the diffusion enhancement factors of electrons and holes, respectively. They are functions of the Fermi-Dirac integrals and allow to generalize the Einstein relation [14], in order to be consistent with both degenerate and non-degenerate semiconductors.

$$g_{n,p} = \frac{\mathcal{F}_{1/2}(\eta_{n,p})}{d\mathcal{F}_{1/2}(\eta_{n,p})/d\eta_{n,p}} \tag{4}$$

In equation (4), the quantities $\eta_n = \frac{E_{fn} - E_c}{kT}$ and $\eta_p = \frac{E_v - E_{fp}}{kT}$ are the reduced Fermi energies of electrons and holes. Where E_c and E_v are the conduction and valence band edges, respectively. The quasi-Fermi levels of electrons $E_{fn} = -q\varphi_n$ and holes $E_{fp} = -q\varphi_p$ are functions of the quasi-Fermi potentials of electrons φ_n and holes φ_p. The function $\mathcal{F}_{1/2}$ is the half Fermi-Dirac integral, which we use also to calculate the electrons and holes densities, whose expressions are given in equations (5) and (6).

$$n = N_c \mathcal{F}_{1/2}(\eta_n) \tag{5}$$

$$p = N_v \mathcal{F}_{1/2}(\eta_p) \tag{6}$$

Where N_c and N_v are the band effective densities of states in the conduction and valence bands, respectively. To simulate semiconductors, we need to solve the continuity equations of carriers (7) and (8), which are coupled with the Poisson equation (9).

$$\frac{dJ_n}{dx} + q(G - R) = 0 \tag{7}$$

$$\frac{dJ_p}{dx} - q(G - R) = 0 \tag{8}$$

$$\frac{d^2 V}{dx^2} + \frac{q}{\varepsilon}(p - n + N_d^+ - N_a^- + p_t - n_t) = 0 \tag{9}$$

Where ε is the dielectric constant of the material and q is the elementary charge. N_d^+ and N_a^- are the densities of ionized donor and acceptor atoms. The densities of trapped holes p_t and trapped electrons n_t are calculated by

using the Shockley-Read-Hall (SRH) statistics [16,17]. In the continuity equations, the term G refers to the generation rate and R *is* the recombination rate of electrons and holes. Our model takes into account the radiative and Auger recombination process whose expressions are given, respectively, in equations (10) an (11).

$$R_{rad} = \beta_{rad}\left(np - n_i^2\right) \tag{10}$$

$$R_{auger} = \left(\beta_{auger,n}n + \beta_{auger,p}p\right)\left(np - n_i^2\right) \tag{11}$$

Where n_i is the intrinsic concentration and β_{rad} is the radiative recombination coefficient. $\beta_{auger,n}$ and $\beta_{auger,p}$ are the Auger recombination coefficients of electrons and holes, respectively.

2.2. *Tunneling models*
In addition to the classical transport processes (drift and diffusion), tunneling of carriers through the bandgap has to be taken into account in highly doped semiconductor structures. As it is shown in Figure 1, this effect can be direct (band-to-band tunneling BBT) or via traps (traps-assisted tunneling TAT). In this figure, E_c and E_v are the conduction and valence band edges, respectively. E_{fr} and E_{fl} are the Fermi levels in the right and left quasi-neutral sides of the pn-junction, respectively. E_t is the energy level corresponding to the trap. E_{cm} and E_{vm} are conduction and valence band extreme, respectively. By adding these two mechanisms, the total recombination rate is given by the equation (12).
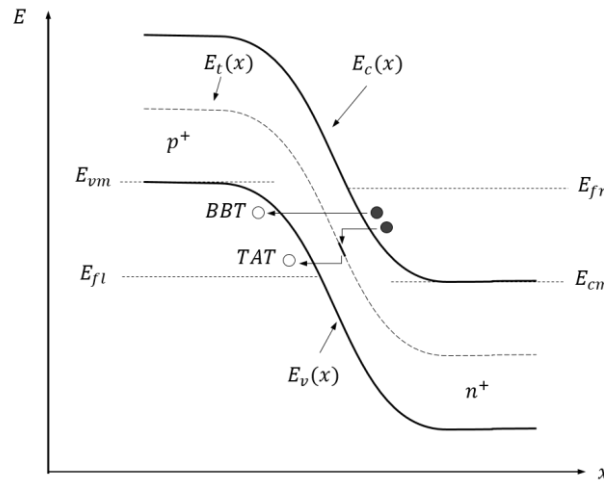
Figure 1: Schematic of BBT and TAT in a degenerate pn-junction.

$$R = R_{rad} + R_{auger} + R_{bbt} + R_{tat} \tag{12}$$

Where R_{bbt} is the band-to-band tunneling contribution and R_{tat} is the contribution of transitions via traps. Depending on the type of the trap, which can be donor-like or acceptor-like, the traps-assisted tunneling is the sum of two components ($R_{tat} = R_{tat,a} + R_{tat,d}$), as it will be shown later.

2.3. *Band-to-band tunneling model*
As it has been shown in equation (12), this mechanism can be incorporated in the drift-diffusion model by means of an additional recombination term into the continuity equations. It is described by the Esaki formalism [18] and the corresponding recombination term for an energy level E, is given by

$$R_{bbt} = \frac{4\pi q k_b T}{h^3} \, F \, T_c \left[m_n^* log\left(\frac{1 + exp\left(\frac{E_{fn1}-E}{k_b T}\right)}{1 + exp\left(\frac{E_{fn2}-E}{k_b T}\right)}\right) - m_h^* log\left(\frac{1 + exp\left(\frac{E_{fp1}-E}{k_b T}\right)}{1 + exp\left(\frac{E_{fp2}-E}{k_b T}\right)}\right) \right] \tag{12}$$

Where h is the Planck's constant and F is the local electric field. m_n^* and m_n^* are the effective masses of electrons and holes, respectively. T_c is the tunneling probability for a carrier tunneling from one side to another one. Using the Wentzel–Kramers–Brillouin (WKB) approximation [16], the expression of this probability is given in equation (13). The logarithmicterm, in equation (12), describes the supply function of carriers.

$$T_c = exp\left(-\frac{4\sqrt{2m_{tun}E_g^3}}{3q\hbar|F|}\right) \tag{13}$$

Here, $m_{tun} = \frac{m_n^* m_h^*}{m_n^* + m_h^*}$ is the effective tunneling mass, E_g is the bandgap energy and $\hbar$ is the reduced Planck's constant.

2.3.1 *traps-assisted tunneling model*
This tunneling component is dominant at high electric fields and can modify the characteristics of the device. It is modeled by including appropriate enhancement factors (Γ_n and Γ_p) [19] to modify the electron and hole capture cross sections (σ_n and σ_p) in the SRH statistics.

For donor-like traps of density N_{td} and energy E_{td}, present within the bandgap, the net transition rate and density of trapped holes are given in equations (15) and (16), respectively.

$$R_{tat,d} = N_{td} \frac{(1+\Gamma_n)\sigma_{nd}(1+\Gamma_p)\sigma_{pd} v_{th}(np - n_i^2)}{(1+\Gamma_n)\sigma_{nd}\left[n + N_c exp\left(-\frac{E_c - E_{td}}{k_bT}\right)\right] + (1+\Gamma_p)\sigma_{pd}\left[p + N_v exp\left(\frac{E_v - E_{td}}{k_bT}\right)\right]} \tag{14}$$

$$p_t = N_{td} \frac{\left(1+\Gamma_p\right)\sigma_{pd} p + (1+\Gamma_n)\sigma_{nd} N_c exp\left(-\frac{E_c - E_{td}}{k_bT}\right)}{(1+\Gamma_n)\sigma_{nd}\left[n + N_c exp\left(-\frac{E_c - E_{td}}{k_bT}\right)\right] + \left(1+\Gamma_p\right)\sigma_{pd}\left[p + N_v exp\left(\frac{E_v - E_{td}}{k_bT}\right)\right]} \tag{15}$$

While for acceptor-like traps of density N_{ta} and energy E_{ta}, the net transition rate and trapped electrons density are given in equations (17) and (18),respectively.

$$R_{tat,a} = N_{ta} \frac{(1+\Gamma_n)\sigma_{na}(1+\Gamma_p)\sigma_{pa} v_{th}(np - n_i^2)}{(1+\Gamma_n)\sigma_{na}\left[n + N_c exp\left(-\frac{E_c - E_{ta}}{k_bT}\right)\right] + (1+\Gamma_p)\sigma_{pa}\left[p + N_v exp\left(\frac{E_v - E_{ta}}{k_bT}\right)\right]} \tag{16}$$

$$n_t = N_{ta} \frac{(1+\Gamma_n)\sigma_{na} n + \left(1+\Gamma_p\right)\sigma_{pa} N_v exp\left(\frac{E_v - E_{ta}}{k_bT}\right)}{(1+\Gamma_n)\sigma_{na}\left[n + N_c exp\left(-\frac{E_c - E_{ta}}{k_bT}\right)\right] + (1+\Gamma_p)\sigma_{pa}\left[p + N_v exp\left(\frac{E_v - E_{ta}}{k_bT}\right)\right]} \tag{17}$$

The field enhancement factors Γ_n for electrons and Γ_p for holes are defined in equation (19).

$$\Gamma_{n,p} = \frac{\Delta E_{n,p}}{k_bT}\int_0^1 \exp\left(\frac{\Delta E_{n,p}}{k_bT}u - \frac{4\sqrt{2\Delta E_{n,p}^3}}{3q\hbar|F|}u^{3/2}\right)du \tag{18}$$

In this equation, the quantities ΔE_n and ΔE_p represent the ranges of energies from which the tunneling is possible. It is assumed that the tunneling of electrons, from conduction band, is possible only for energies above the trap level. While tunneling of holes, from valence band, occurs only for energies below the trap level. The widths of theserangesare given in equations (20) and (21).

$$\Delta E_n = \begin{cases} E_c(x) - E_{cm} & E_t(x) \leq E_{cm} \\ E_c(x) - E_t(x) & E_t(x) > E_{cm} \end{cases} \tag{19}$$

$$\Delta E_p = \begin{cases} E_{vm} - E_v(x) & E_t(x) > E_{vm} \\ E_t(x) - E_v(x) & E_t(x) \leq E_{vm} \end{cases} \tag{20}$$

Where E_{cm} and E_{cm} are the extreme values of conduction band and valence band, as it was shown in Figure 1.

3. Results and discussion

The model described above was discretized using the finite differences method. The domain was partitioned into sub-regions by a variable mesh, which becomes smaller near to junctions between layers and metallic contacts at boundaries. This discretization leads to a nonlinear problem with the state variables V, φ_n and φ_p at principal nodes (N). An extended Scharfetter-Gummel scheme (22) and (23) was used to decouple the transport equations and evaluate the current densities in the secondary nodes ($M = N + 1/2$). The metallic contacts at boundaries were chosen such that contact barriers are zeros in order to have good ohmic contacts.

$$J_{n,M} = \frac{k_b T \mu_{n,M}}{h_N} g_{n,M} \left[B\left(\frac{V_{N+1} - V_N}{\frac{k_b T}{q} g_{n,M}} \right) n_{N+1} - B\left(\frac{V_N - V_{N-1}}{\frac{k_b T}{q} g_{n,M}} \right) n_N \right] \tag{21}$$

$$J_{p,M} = \frac{k_b T \mu_{p,M}}{h_N} g_{p,M} \left[B\left(\frac{V_{N+1} - V_N}{\frac{k_b T}{q} g_{p,M}} \right) p_N - B\left(\frac{V_N - V_{N-1}}{\frac{k_b T}{q} g_{p,M}} \right) p_{N+1} \right] \tag{22}$$

In both equations (22) and (23),h_N is the length of spacing mesh and $B(z) = \frac{z}{\exp(z)-1}$ is the Bernoulli function. g_n and g_p are the diffusion enhancement factors given in equation (4).

Our model was simulated on a multijunction structure whose layer system characteristics are given in Table (1). Itcontains eight layers with a total thickness of 1059 nm. It includes layers with different levels of doping and a degenerate pn-GaAs junction.

Table 1: Nominal thicknesses and doping concentrations of the investigated test structure [20].

Material	Thickness (nm)	Doping concentration (cm^{-3})
GaAS	300	$N_a = 7.5 \times 10^{18}$
GaAS	300	$N_a = 2.5 \times 10^{18}$
$Al_{0.3}Ga_{0.7}As$	30	$N_a = 3.2 \times 10^{18}$
GaAS	28	$N_a = 3.6 \times 10^{19}$
GaAS	26	$N_d = 1.3 \times 10^{19}$
$Ga_{0.51}In_{0.49}P$	30	$N_d = 7.1 \times 10^{18}$
GaAS	345	$N_d = 4.5 \times 10^{18}$
GaAS	300	$N_d = 2.3 \times 10^{18}$

The doping profile of this structure is shown in Figure 2, where N_d^+ and N_a^- are the concentrations of ionized donors and acceptors, respectively.
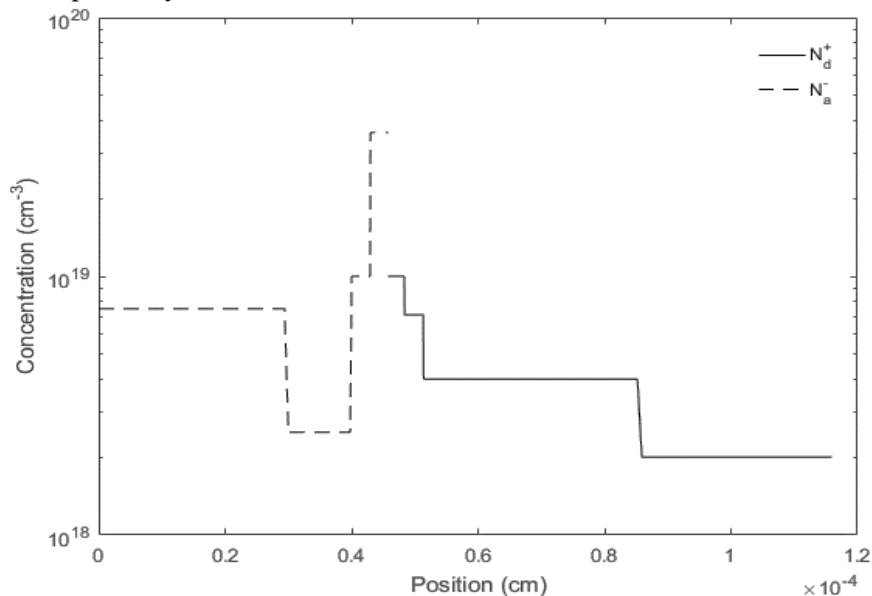
Figure 2: Doping profile of the simulated test structure.

Figure 3 represents the corresponding energy band diagram in thermal equilibrium at zero bias. It shows that the quasi-Fermi levels are overlapped and form a constant level E_f across the layers. This level is inside the band gap for nondegenerate semiconductors, whereas it is inside a permitted band for degenerate semiconductors (it is above E_c for n-type semiconductor and bellow E_v for p-type semiconductor).
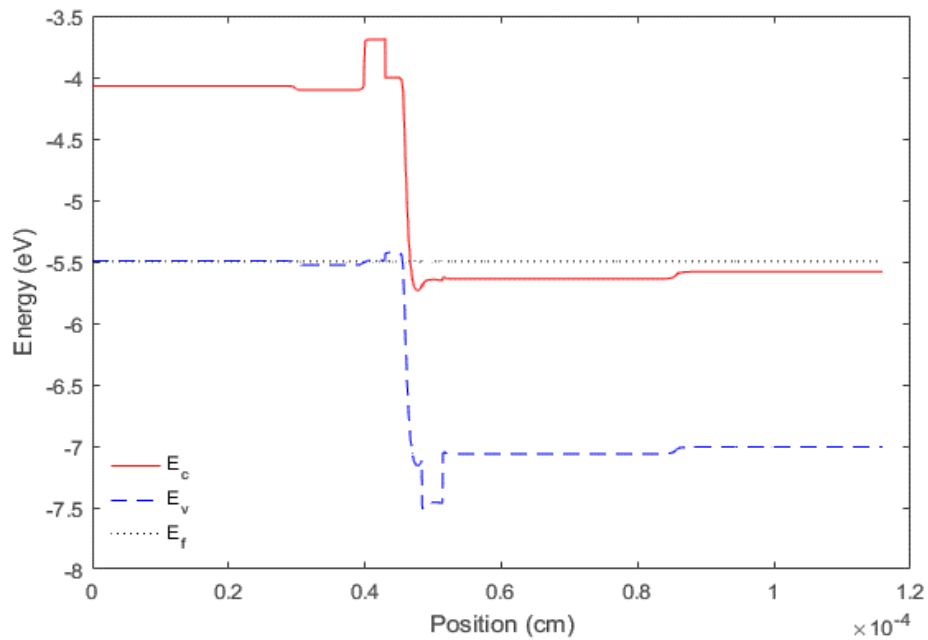
Figure 3: Energy band diagram of the simulated test structure in equilibrium at 0 V bias.

The J-V Characteristic of the simulated test structure is generated by sweeping the voltage from -0.05 V to 0.74 V. As it is shown in Figure 4, in the presence of the band-to-band tunneling model, the J-V curve presents a nominal peak current of 394 A.cm^{-2} for a voltage of 0.16 V and valley current of 133,70 A.cm^{-2} for a voltage of 0.53 V. It is shown also that the traps-assisted tunneling model increases the current density, especially in the range between 0.02 V and 0.64 V.
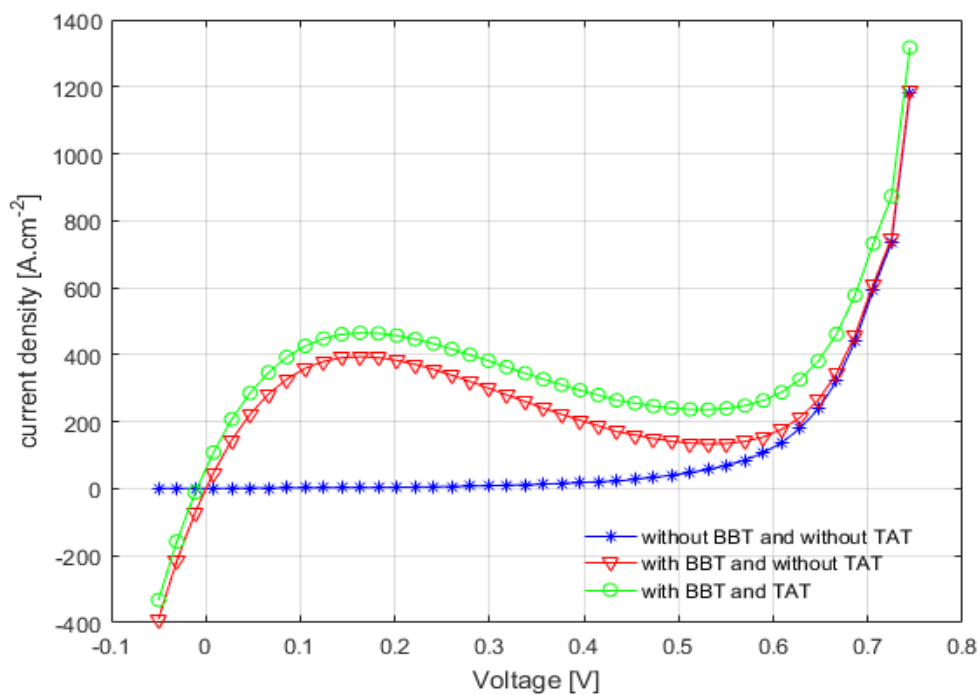
Figure 4: Influence of tunneling models on the J-V characteristic.

Conclusions

The present paper investigated different numerical models for the simulation of tunneling effects in a multijunction structure. The developed model was derived on the drift-diffusion equation by incorporating additional recombination terms in the continuity equations. The BBT effect was modeled using the Esaki formalism, while the TAT was based on the SRH statistics with field effect enhancement factors. Results show that both mechanisms BBT and TAT modify the J-V curve of the device.

References

1. Cotal H., Fetzer C., Boisvert J., Kinsey G., King R., Hebert P., Yoon H., Karam N., *Energy Environ. Sci.,* 2 (2009) 174-192.
2. Kane E. O., *J. Appl. Phys.,* 32 (1961) 83-91.
3. Sze S. M., Ng K. K., *J. Sons*., 3 (2006) 28-50.
4. Hurkx G. A. M., Klaassen D. B. M., Knuvers M. P. *G.*, O'Hara F. G., *IEDM,* 6(1989) 307-310.
5. Baudrit M., Algora V., *WCPEC,* 4 (2006) 826-829.
6. Baudrit M., Algora C., Rey-Stolle I., Garcia I., Galiana B., *NUSOD,* 5 (2005) 41-42.
7. Orazem M., *AIChE Journal,* 32 (1986) 765-772.
8. Benaichi M., Hadrami M, Karkri A.,Chetouani A., *ICEIT,* 2 (2016) 516-520.
9. Blakemore J. S., *Solid-State Electron*., 25 (1982) 1067-1076.
10. Aymerich-Humet X., Serra-Mestres F., Millan J., *J. App. Phys*., 54 (1983) 2850-2851.
11. Kulikovsky A. A., *J. Comput. Phys.,* 119 (1995) 149-155.
12. Koprucki T., Gartner K., *Opt. Quant. Elects*., 45 (2013) 791-796.
13. Koprucki M. K. Fuhrmann T., J., Gartner K, *NUSOD,* 14 (2014) 155-156.
14. Koprucki T., Rotundo N., Farrell P., Doan D., Fuhrmann J., *Opt. Quant. Elects*., 47 (2014) 1327-1332.
15. Karkri A., Hadrami M, Benaichi M.,Chetouani A., *ICEIT,* 2 (2016) 255-259.
16. Hall N., *Phys. Rev*. 87 (1952) 387.
17. Shockley W., Read W. T., *Phys. Rev*., 87 (1952) 835-842.
18. Esaki L., *Phys. Rev.,* 109-603 (1958) 603-604.
19. Hurkx G. A. M., Klaassen D. B. M., Knuvers M. P. G., *Trans. Electron. Devices,* 39 (1992) 2090-2098.
20. Hermle M., Philipps S. P., Letay G., Bett A. W., *Photovolt. Res. Appl*., 16 (2008) 409-418.

(2017) ; http://www.jmaterenvironsci.com